Controlling Amplitudes in 2.5D common-shot migration to zero offset

J. Schleicher and C. Bagaini

email: *js@ime.unicamp.br*

keywords: *Configuration transform, dip moveout, DMO, Kirchhoff-type imaging, true amplitude*

ABSTRACT

Configuration transform operations such as dip moveout, migration to zero offset, shot and offset continuation use seismic data recorded with a certain measurement configuration to simulate data as if recorded with other configurations. Common-Shot Migration to Zero Offset (CS-MZO), analysed in this paper, transforms a common-shot section into a zero-offset section. It can be realized as a Kirchhoff-type stacking operation for 3D wave propagation in a 2D laterally inhomogeneous medium. By application of a suitable weight function, data amplitudes are preserved or transformed by replacing the geometrical-spreading factor of the input reflections by the correct one of the output zero-offset reflections. The necessary weight functions can be computed via 2D dynamic ray tracing in a given macro-velocity model without any a-priori knowledge regarding the dip or curvature of the reflectors. We derive the general expression of the weight function in the general 2.5D situation and specify its form for the particular case of constant velocity. A numerical example validates the expressions and highlights the differences between amplitude preserving and true-amplitude CS-MZO.

INTRODUCTION

Configuration transforms like dip-moveout correction (DMO), migration to zero-offset (MZO), shot or offset continuation (SCO and OCO), and azimuth-moveout correction (AMO) have become a field of great interest in exploration seismics. The objective of a configuration transform is to simulate a seismic section as if obtained with a certain measurement configuration using the data recorded with another configuration. This type of imaging process is not only useful in the seismic processing chain for an improved stack, i.e., for data reduction and signal-to-noise enhancement, but also for wave-equation-based trace interpolation to reconstruct missing data and for velocity analysis. There are quite a number of publications in the area that demonstrate the use of configuration transforms for these purposes, e.g., on MZO and DMO in the common-offset domain[1] (Black et al., 1993; Bleistein and Cohen, 1995; Canning and Gardner, 1996; Collins, 1997; Tygel et al., 1998) or in the common-shot domain (Biondi and Ronen, 1987), OCO (Fomel, 1994; Fomel and Bleistein, 1996; Santos et al., 1997), SCO (Bagaini and Spagnolini, 1996), AMO (Biondi et al., 1996).

In this paper, we investigate another of these configuration transform methods, being Common Shot Migration to Zero-Offset (CS-MZO). Its purpose is to transform a single common shot section into a zero-offset section. This can be realized as a direct one-step procedure or split up into two steps, these being a normal-moveout correction (NMO) plus a subsequent common-shot DMO (CS-DMO). The kinematic properties of the latter process have already been studied by Biondi and Ronen (1987), who also proposed a cost-effective implementation in the log-stretch domain. To further reduce the method's computation time, Cabrera and Levy (1989) and Granser (1994) have suggested approximate versions of the CS-DMO operator. Hearn (1989) pointed out the importance of controlling the weights for a space-time implemen-

[1] MZO is defined in homogeneous media as the cascade of NMO and DMO. In inhomogeneous media, MZO is the more general process that can be split only approximately into NMO and DMO.

tation of CS-DMO and, based on a geometrical analysis, suggested a first amplitude distribution. Here, we derive the correct weights for Kirchhoff CS-DMO and CS-MZO.

The main advantage of the common-shot implementation over the standard one in the common-offset domain is that no data sorting is needed. Moreover, a CS-MZO simulated zero-offset section is obtained from a different subset of the data than a standard one, thus enabling an independent quality control over the velocity information used in the procedure. Here, we discuss the realization of an CS-MZO in form of a Kirchhoff-type stacking operation. Moreover, we address particular features of CS-MZO such as how to control the simulated zero-offset amplitudes by an adequate weight in the Kirchhoff implementation and how to choose the correct operator aperture.

There are two main competing concepts in the seismic imaging literature that receive the designations "amplitude preserving" or "true amplitude". In this paper, we adopt the term "true amplitude" for imaging procedures that treat the input amplitudes in such a way that the geometrical-spreading factors are correctly transformed. We reserve the term "amplitude preserving" for procedures that do not alter the input amplitudes.

In this work, we discuss CS-MZO weights for both types of amplitude processing. With true-amplitude weights, the shot moveout procedure proposed here is designed to produce, from a common-shot section, a simulated zero-offset section that is kinematically and dynamically equivalent to the one obtained from common-offset data using a true-amplitude MZO. In other words, the true-amplitude weight function for CS-MZO acts so that the simulated zero-offset amplitudes are proportional to the ratio between the original angle-dependent common-shot reflection coefficient and the zero-offset geometrical-spreading factor. In this way, these amplitudes are directly comparable to those obtained from a true-amplitude MZO or from modeling a synthetic zero-offset section. On the other hand, with amplitude-preserving weights, spherical-divergence corrected common-shot sections can be transformed to corresponding zero-offset sections so as to directly enable an AVO or AVA analysis in the time domain.

KIRCHHOFF-TYPE CS-MZO

Like conventional MZO in the common-offset domain, also CS-MZO is based on the general 3D Kirchhoff-type formula for configuration transforms of Tygel et al. (1996), who discuss a unified approach to amplitude-preserving seismic reflection imaging for 3D seismic records with an arbitrary measurement configurations and laterally and vertically inhomogeneous, isotropic macrovelocity models. Here, we consider a 2.5D situation, i.e., 3D wave propagation in a 2D (isotropic, vertically and laterally inhomogeneous) earth model. There exist no medium variations in the out-of-plane y-direction perpendicular to the seismic line. In particular, all reflectors can be specified by in-plane (x, z)-curves. Moreover, all point sources, assumed to omnidirectionally emit identical pulses, and all receivers, assumed to have identical characteristics, are distributed along the x-axis so that only in-plane propagation needs to be considered. For the 2.5D problem, the full 3D geometrical-spreading factor of an in-plane ray can be written as product of in-plane and out-of-plane factors (Bleistein, 1986). Both quantities can be computed using 2D dynamic ray tracing (Červený, 1987, 2001).

Let the original (input) common-shot measurement configuration be parameterized by the (fixed) source coordinate s and the (variable) half-offset coordinate h (see Figure 1). On the measurement surface $z = 0$ and along the seismic line $y = 0$, these coordinates define the locations of the fixed source at $S = (s, 0, 0)$ and the corresponding receivers at $G = G(h) = (g, 0, 0)$, where $g = s + 2h$. At each receiver position G, a scalar wavefield induced by the corresponding point source at S is recorded. The output zero-offset configuration is parametrized by the coordinate s_0 that describes coincident source-receiver pairs at $S_0(s_0) = G_0(s_0) = (s_0, 0, 0)$.

In the following, we assume that each (real) seismic trace in the input section has already been transformed into its corresponding analytic (complex) trace by adding the Hilbert transform of the original trace as imaginary part[2]. Therefore, the output common-offset section will be also considered analytic. The analytic traces of the input section will be denoted by $U(h, t)$, where t is the time coordinate of the common-shot section. Correspondingly, the analytic traces of the output section will be denoted by $U_0(s_0, t_0)$, where t_0 is the time coordinate of the simulated zero-offset section.

[2]Like for other Kirchhoff procedures, the analytic traces are needed to account for caustics along the ray path and to correctly recover complex reflection coefficients.

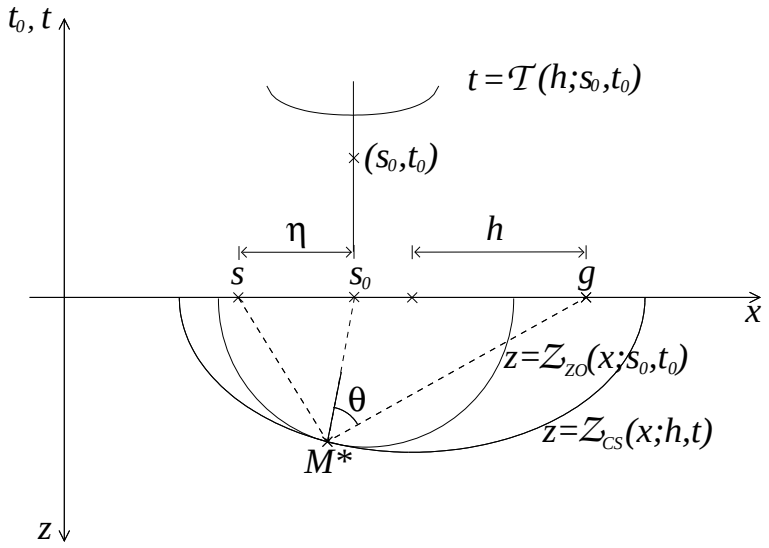

Figure 1: Geometrical properties of a common-shot MZO. Depicted are the common-shot and zero-offset isochrons $z = \mathcal{Z}_{CS}$ and $z = \mathcal{Z}_{ZO}$. Their tangency point M^* defines the CS-MZO stacking line $\mathcal{T}$ as a function of half-offset h for a given point (s_0, t_0).

Stacking integral

For each point (s_0, t_0) in the output zero-offset section to be simulated, the stack result $U_0(s_0, t_0)$ will be obtained by means of a weighted stack of the input data, represented by the following integral

$$U_0(s_0,t_0) = \frac{1}{\sqrt{2\pi}} \int_A dh\; \mathcal{W}(h; s_0, t_0)\; D_-^{1/2}[U(h,t)]\Big|_{t=\mathcal{T}(h;s_0,t_0)} \quad . \tag{1}$$

Similarly to the situation in other familiar 2.5D Kirchhoff-type imaging procedures like migration (Bleistein et al., 1987; Martins et al., 1997), DMO (Black et al., 1993), OCO (Santos et al., 1997), or MZO (Tygel et al., 1998), the input traces $U(h, t)$ are to be weighted by a certain factor $\mathcal{W}(h; s_0, t_0)$ and then to be summed up along the stacking line $t = \mathcal{T}(h; s_0, t_0)$. Both functions depend on the point (s_0, t_0) where the stack is to be placed, as well as on the variable h that specifies the traces being considered in the stack. Moreover, A denotes the aperture of the stack, i.e., the range of half-offsets for which data are available in the input section. Finally, the (time-reverse) time half-derivative, given by

$$D_-^{1/2}[f(t)] = \mathcal{F}^{-1}\left[|\omega|^{1/2} \mathrm{e}^{-i\frac{\pi}{4}\mathrm{sign}(\omega)} \mathcal{F}[f(t)]\right] \;, \tag{2}$$

where $\mathcal{F}$ denotes the Fourier transform, is needed to correct the pulse shape. It is a natural 2.5D counterpart (Bleistein et al., 1987) to the full derivative that is part of a full 3D Kirchhoff-type migration scheme (Newman, 1975; Schleicher et al., 1993).

The stacking line $\mathcal{T}$ is defined by the kinematics of the operation, and the weight function $\mathcal{W}$ will be determined by the desired amplitude behaviour. For the true-amplitude weight function, this is achieved by imposing the requirement that, asymptotically, the simulated reflections must have the same geometrical-spreading factor as corresponding true reflections in a zero-offset section. Correspondingly, for the amplitude-preserving weight, the imposed condition is that of unaltered amplitudes. As shown below, the resulting true-amplitude weight function does not depend on any reflector properties. It can be computed for any arbitrary point (s_0, t_0) in the zero-offset section to be simulated using no other information than that provided by the given smooth macrovelocity model.

Stacking line

The stacking line $\mathcal{T}$ is constructed as the *inplanat* (Tygel et al., 1996) for the configuration transform problem, which is defined as the kinematic image in the input section of a point in the output section. To

explain this construction (see also Figure 1 for the constant-velocity case), let us start from a fixed point (s_0, t_0) in the output section and compute the corresponding stacking line. The two-step procedure is:

(i) For the given point (s_0, t_0), draw the isochron in depth, $z = \mathcal{Z}_{ZO}(x; s_0, t_0)$. This isochron is implicitly defined by all depth points $M = (x, \mathcal{Z}_{ZO}(x; s_0, t_0))$ for which the sum of the traveltimes along the two ray segments S_0M and MG_0 connecting M to the source-receiver pair (S_0, G_0), equals the given time coordinate t_0, viz.,

$$\tau(S_0, M) + \tau(M, G_0) = 2\tau(S_0, M) = t_0 \ . \tag{3}$$

These traveltimes $\tau(S_0, M)$ and $\tau(M, G_0)$ are to be constructed in the given macrovelocity model. For constant velocity, the resulting isochron is the lower half-circle with center at $S_0 = G_0$ and radius $R_0 = vt_0/2$.

(ii) Treat the isochron (3) as a reflector and construct its reflection traveltime curve with the input configuration, i.e., compute the reflection traveltimes for all source-receiver pairs (S, G) by forward modeling. The resulting CS-MZO stacking curve may then be written as

$$t = \mathcal{T}(h; s_0, t_0) = \tau(S, M^*) + \tau(M^*, G) \ , \tag{4}$$

where, for each half-offset h, point M^* is the specular reflection point on the isochron $z = \mathcal{Z}_{ZO}(x; s_0, t_0)$ of the source-receiver pair (S, G) specified by h. Point M^*, which is assumed to be unique, has the coordinates $(x^*, \mathcal{Z}_{ZO}(x^*; s_0, t_0))$, where $x^* \equiv x^*(h; s_0, t_0)$ is obtained using the stationarity condition

$$\frac{\partial}{\partial x}(\tau(S_0, M) + \tau(M, G_0))\bigg|_{x=x^*} = 0 \ . \tag{5}$$

In the first section of the Appendix, the CS-MZO stacking line $t = \mathcal{T}(h; s_0, t_0)$ for a constant-velocity medium is actually constructed following the above geometrical prescriptions. It reads

$$\mathcal{T}(h; s_0, t_0) = \frac{2h}{v}\sqrt{1 + \frac{R_0^2}{\eta(2h - \eta)}} \ , \tag{6}$$

where $\eta = s_0 - s$ is the distance between the common source point of the input section and the desired output point (see again Figure 1). This stacking line or inplanat is, of course, equivalent to the smear-stacking ellipse or outplanat

$$\frac{(vt_0)^2}{(vt)^2 - (2h)^2} + \frac{(\eta - h)^2}{h^2} = 1 \tag{7}$$

previously derived by Biondi and Ronen (1987) or Hearn (1989).

We see from equation (6) that a real stacking line exists only if $\eta \neq 0$, $\eta \neq 2h$, and $\dfrac{R_0^2}{\eta(\eta - 2h)} \leq 1$. The first conditions implies that we cannot construct a zero-offset trace at the source position. The second condition means that for the construction of the zero-offset trace at a distance of η from the source, the trace recorded at this position must not enter the stack. The requirement of a continuous and smooth stacking line together with the third of the above conditions already provides a first condition for the aperture A of stack (1). Certainly, only half-offsets $0 < h < \eta/2$ or $h > \eta/2$ will enter the stack. We will see later that the aperture actually needed is even smaller.

Weight function

Analogously to the above, we now consider the isochron of a point (h, t) in the input section, this isochron being supposed to exist and being parameterized in the form $z = \mathcal{Z}_{CS}(x; h, t)$. For constant velocity, this is the lower half-ellipse with foci at S and G and semi-axes $a = vt/2$ and $b = \sqrt{a^2 - h^2}$. The isochron $z = \mathcal{Z}_{CS}(x; h, t)$ is tangent to the isochron $z = \mathcal{Z}_{ZO}(x; s_0, t_0)$ at M^* for arbitrarily heterogeneous macrovelocity models.

Let us now denote the 3D point-source geometrical spreading factors for the ray segments SM^* and M^*G by $\mathcal{L}_S$ and $\mathcal{L}_G$, respectively. Correspondingly, we denote the 3D point-source geometrical spreading factors for the ray segments S_0M^* and M^*G_0 by $\mathcal{L}_0$. Also, the velocity at M^* is denoted by v^*. Moreover, let θ denote the incident angle between the ray SM^* and the isochron normal at M^*. Note that this is half the angle between the ray segments SM^* and M^*G. We also need the in-plane curvatures K and K_0 of the isochrons $z = \mathcal{Z}_{CS}(x;h,t)$ and $z = \mathcal{Z}_{ZO}(x;s_0,t_0)$, respectively, at M^*. In homogeneous media, the latter is a circle with curvature $K_0 = -1/R_0$ (see Figure 1). Furthermore, the out-of-plane Fresnel geometrical-spreading factors (Tygel et al., 1994) of the rays SMG and S_0MG_0 are denoted by $\mathcal{L}_F$ and $\mathcal{L}_{F0}$, respectively. Finally, let h_B be the 2D Beylkin determinant (Beylkin, 1985; Bleistein, 1987; Tygel et al., 1995). With the help of these quantities, the true-amplitude weight function $\mathcal{W}^{TA}(h;s_0,t_0)$ can be expressed as

$$\mathcal{W}^{TA}(h;s_0,t_0) = \left(\frac{v^*}{2}\right)^{3/2} \frac{\mathcal{L}_S\mathcal{L}_G}{\mathcal{L}_0^2}\frac{\mathcal{L}_{F0}}{\mathcal{L}_F}\frac{1}{\cos^2\theta}\frac{|h_B|}{\sqrt{|K-K_0|}}\exp\{i\frac{\pi}{2}\kappa\}\ , \tag{8}$$

where $\kappa = (1-\mathrm{sign}(K-K_0))/2$. The derivation of expression (8) is virtually identical to that of the true-amplitude weight function for common-offset MZO (Tygel et al., 1998, see their Appendix A) and is thus omitted here.

As shown in the Appendix, the true-amplitude CS-MZO weight function (8) reduces for a constant velocity v to

$$\mathcal{W}^{TA}(h;s_0,t_0) = \sqrt{\mathcal{T}}\sqrt{\frac{\eta}{(2h-\eta)^3}}\ . \tag{9}$$

For an amplitude-preserving CS-MZO, i.e., one that does not alter peak amplitudes of reflections from planar reflectors, the weight function reads

$$\mathcal{W}^{AP}(h;s_0,t_0) = \frac{t_0}{\sqrt{\mathcal{T}}}\sqrt{\frac{\eta}{(2h-\eta)^3}}\ . \tag{10}$$

If the CS-MZO operation (1) is applied to a NMO corrected common-shot section, i.e., as a common-shot DMO, the stacking line and the weight function must be modified. The CS-DMO stacking line is obtained from an NMO correction of the CS-MZO stacking line,

$$t_n = \widetilde{\mathcal{T}}(h,s_0,t_0) = \sqrt{\mathcal{T}^2 - 4h^2/v^2} = \frac{t_0\,h}{\sqrt{\eta(2h-\eta)}}\ , \tag{11}$$

where t_n is the time coordinate of the NMO corrected common-shot section. The true-amplitude CS-DMO weight function is

$$\widetilde{\mathcal{W}}^{TA}(h;s_0,t_0) = \frac{\sqrt{\widetilde{\mathcal{T}}^2 + 4h^2/v^2}}{t_0}\sqrt{\widetilde{\mathcal{T}}}\,\frac{\eta}{h(2h-\eta)}\ , \tag{12}$$

and the one for an amplitude-preserving CS-DMO reads

$$\widetilde{\mathcal{W}}^{AP}(h;s_0,t_0) = \sqrt{\widetilde{\mathcal{T}}}\,\frac{\eta}{h(2h-\eta)}\ . \tag{13}$$

Note that the above weight functions are to be used if the half derivative in the CS-DMO is applied with respect to the NMO corrected traveltime t_n. In many practical implementations of DMO, however, this derivative is taken with respect to the output zero-offset traveltime t_0. In this case, the above weight functions need to be slightly modified. Then, the true-amplitude CS-DMO weight function reads

$$\widetilde{\mathcal{W}}_0^{TA}(h;s_0,t_0) = \frac{\sqrt{\widetilde{\mathcal{T}}^2 + 4h^2/v^2}}{\sqrt{t_0}}\,\frac{\eta}{h(2h-\eta)}\ , \tag{14}$$

and the amplitude-preserving CS-DMO weight function is

$$\widetilde{\mathcal{W}}_0^{AP}(h;s_0,t_0) = \sqrt{t_0}\,\frac{\eta}{h(2h-\eta)}\ . \tag{15}$$

The weight function of equation (15) is the CS-DMO equivalent to the one of Black et al. (1993) for a standard common-offset DMO.

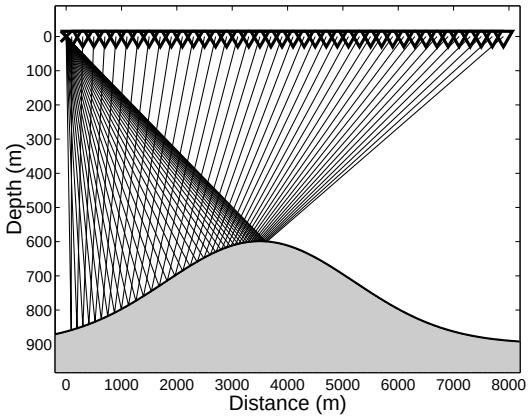

Figure 2: Earth model for the numerical experiment. Also shown is the ray family for the modeled common-shot experiment.

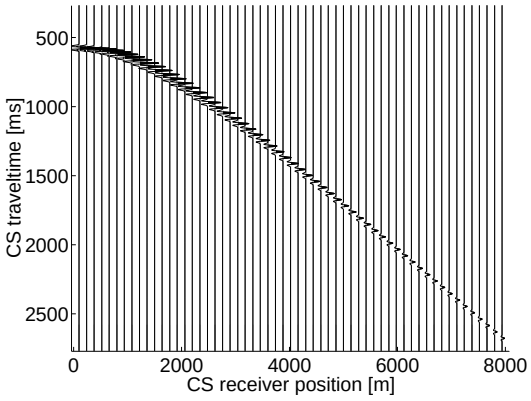

Figure 3: Ray-synthetic common-shot data for the numerical experiment.

Comparison to Hearn's weight

Based on a geometrically appealing discussion of amplitudes, Hearn (1989) has already suggested an amplitude-preserving CS-DMO weight function. However, a simple dimension analysis shows that it cannot be correct. Here, we compare it numerically to the above expressions. For that purpose, we rewrite it in our notation. With the help of the formulas in the Appendix, Hearn's weight can be represented as

$$\tilde{\mathcal{W}}_H^{AP} = \sqrt{\frac{(2R_0^2(1+\rho) - h^2\rho^2)(R_0^2(1+\rho) - h^2\rho^2)}{2R_0(R_0^2 + h^2 - (h-\eta)^2)^3}} \,, \tag{16}$$

where ρ is given by equation (25).

CS-MZO aperture

The basic condition for the aperture is the existence of the stationary point of integral (1). For constant velocity, this condition is discussed in detail in the Appendix. It results in the following condition for h

$$\begin{aligned} \frac{\eta(R_0+\eta)}{R_0+2\eta} < h < \frac{\eta(R_0-\eta)}{R_0-2\eta} \qquad & \text{for } \eta < R_0/2 \,, \\ h > \frac{\eta(R_0+\eta)}{R_0+2\eta} \qquad & \text{for } \eta \geq R_0/2 \,. \end{aligned} \tag{17}$$

The left-hand side expression in inequality (17) is always larger than $\eta/2$ but smaller than η. The alternative condition that the maximum time dip must not exceed $1/v$ yields the same aperture condition (17).

Condition (17) means that for large η, i.e., zero-offset traces far away from the source, an infinite offset is needed, while for small η, i.e., zero-offset traces relatively close to the source position, the stack (1) is carried out over a finite aperture. It is important to note that the CS-MZO aperture may even reduce to very few traces, thus becoming prohibitively small. As a Kirchhoff operation, CS-MZO needs sufficient traces to guarantee interference in the stack (1). Where this cannot be achieved, the aperture should be reduced to include only the one single trace at $h = \eta$, and the weight factor and the half-derivative should be omitted.

NUMERICAL EXPERIMENT

To verify the validity of the CS-MZO weight function (8), we use a simple synthetic example. The model is shown in Figure 2. It consists of two homogeneous acoustic half-spaces separated by a smoothly curved interface. The velocities above and below the interface are 3 km/s and 3.5 km/s, respectively. For this model, we have simulated by ray tracing a common-shot experiment with 396 receivers, the first being

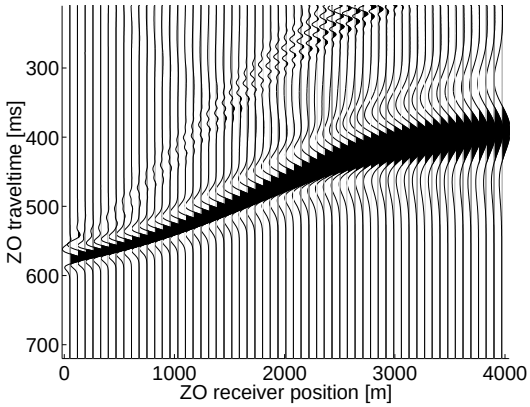

Figure 4: Result of a CS-MZO with true-amplitude weights applied to the data of Figure 3.

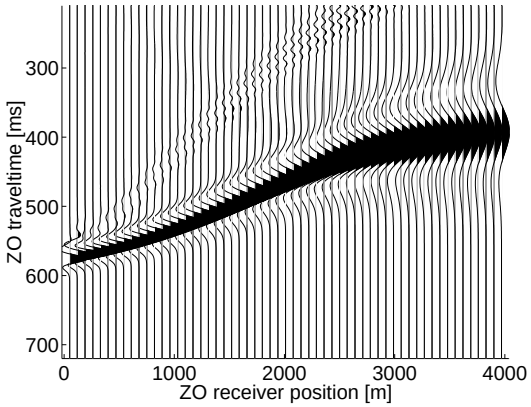

Figure 5: Result of a CS-MZO with amplitude preserving weights applied to the data of Figure 3.

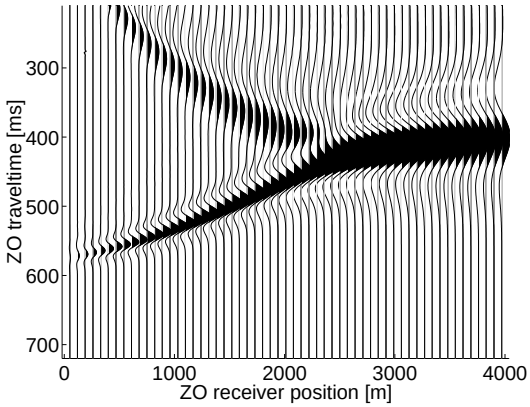

Figure 6: Result of a CS-MZO with no (i.e., unit) weights applied to the data of Figure 3.

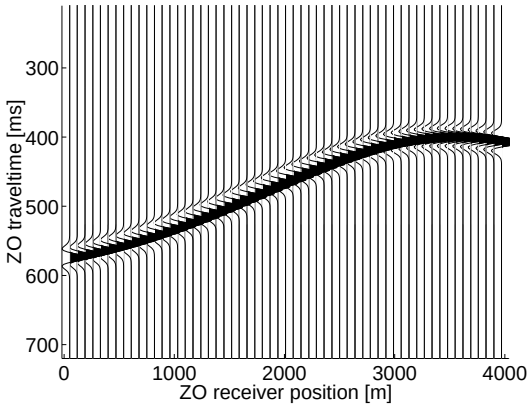

Figure 7: Synthetic zero-offset section for the model in Figure 2.

located at an offset of 100 m from the source. Receiver spacing was 20 m and the time sampling interval was 2 ms. The obtained common shot gather is represented in Figure 3, in which every seventh trace is shown.

To test our analytic results, we have applied the common shot MZO with the proposed weights to the modeled common-shot data. The resulting simulated zero-offset sections are depicted in Figure 4 to 6. Figure 4 shows the result of a CS-MZO using the true-amplitude weight (9). Figure 5 shows the result of a CS-MZO using the amplitude-preserving weight (10). Of course, prior to the application of the latter, the data of Figure 3 have been scaled by vt. For comparison, Figure 6 shows the result of a CS-MZO using a unit weight.

The quality of the obtained results can be checked best by a comparison to a modeled zero-offset section. Therefore, we have also simulated by ray tracing a zero-offset experiment with 396 receivers, equally spaced at every 10 m, beginning at 50 m from the original source. The resulting modeled zero-offset section is depicted in Figure 7. For better comparison between the amplitudes of the simulated and modeled common-offset sections, we refrained from using the correct angle-dependent reflection coefficient in the modeling but computed the common-offset and zero-offset reflections with a constant unit reflection coefficient. In this way, the simulated common-offset amplitudes after a true-amplitude CS-MZO should ideally be identical to those obtained from modeling.

Visual inspection of the simulated and modeled zero-offset sections permits some preliminary qualitative observations. The first impression of the simulated zero-offset sections of Figures 4 to 6 is mainly influenced by the strongly varying pulse length along the reflection event. This is due to the well-known

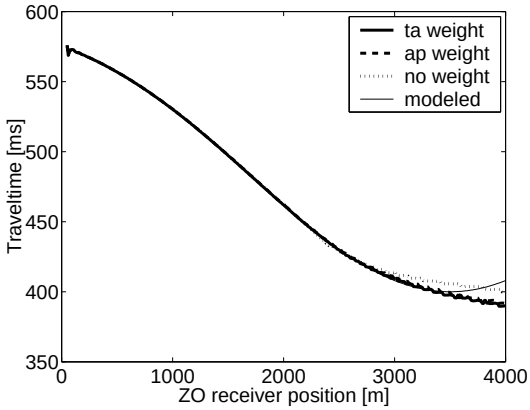

Figure 8: Picked traveltimes of the simulated and modeled zero-offset reflections of Figures 4 to 7.

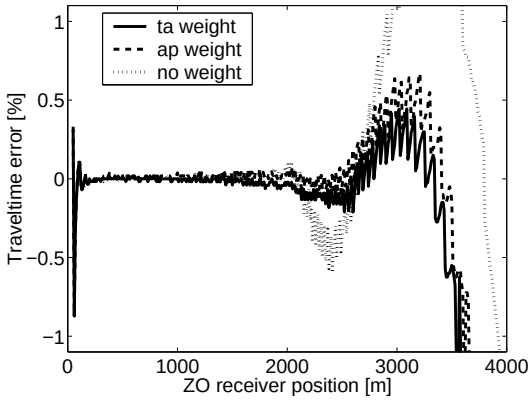

Figure 9: Traveltime error of the simulated zero-offset reflections as compared to the modeled ones.

fact that independently of any possible weights, configuration transformations do not reproduce the bandwidth of the modeled data. Like in the case of common-offset MZO, the pulse stretch is given by the cosine of the reflection angle (Fomel and Bleistein, 1996; Tygel et al., 1998).

Apart from the stretch effect, the general impression of the simulated zero-offset reflections is more or less the same in all figures. The shapes of all three simulated zero-offset reflections closely resemble the modeled one. The major differences lie in the different forms of the operator edge effects in the weighted and unweighted sections. While the unweighted CS-MZO has produced a strong "CS-MZO smile" (see Figure 6), the weighted CS-MZOs present a much weaker effect in the form of a dipping precursor to the simulated reflections (see Figure 4).

To enable a more quantitative analysis, the traveltimes and peak amplitudes along the simulated and modeled zero-offset reflections have been picked. The traveltimes are depicted in Figure 8. We see that the kinematic properties of the suggested Kirchhoff CS-MZO are almost perfect up to an offset of about 3000 m. Further away from the source, the input data are insufficient to correctly simulate zero-offset traces. However, the weighted CS-MZO schemes produce correct traveltimes for slightly larger offsets than the unweighted version. This observation can be confirmed in Figure 9 which depicts the relative error of the traveltimes as compared to the modeled zero-offset reflections of Figure 7. Where the data coverage is sufficient, the error is of the order of a tenth of a per cent.

The quality of the amplitudes along the simulated zero-offset reflections of Figures 4 to 6 is discussed with the help of the next figures. Figure 10 compares the amplitudes obtained with a true-amplitude CS-MZO to those of the modeled section. The amplitudes are quite well recovered within the region between about 300 m and 2100 m, which is not affected by boundary effects. Within this region, the amplitude error is less than one per cent, as can be seen in Figure 11. The size of left boundary region can be reduced by a two-trace taper function (dashed line). In our tests, larger tapers did not improve the quality of the image but resulted in stronger precursors.

Figure 12 shows the amplitudes obtained with the amplitude preserving CS-MZO, together with the desired result, which in this case is just a unit amplitude. Except for the boundary regions, the amplitude preservation works quite will even though the reflector is slightly curved. The amplitude error is depicted in Figure 13. Because of the curved reflector, the error is modestly larger than that of true-amplitude CS-MZO (see Figure 11), ranging at about two per cent. The amplitude error will be the larger the stronger the target reflector is curved.

For comparison, Figure 14 shows the amplitudes after an unweighted CS-MZO. In consistency with Hearn (1989), we observe that unweighted CS-MZO amplitudes increase with increasing distance from the original source. Moreover, not only the shape of the curve is different from the desired one (see Figure 10) but also the scale is completely wrong.

Finally, Figure 15 shows the amplitudes as obtained with Hearn's weight. Note that these amplitudes

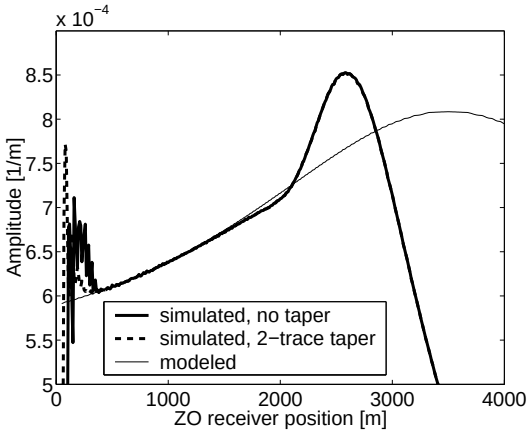

Figure 10: Picked amplitudes of the simulated zero-offset reflections resulting from a true-amplitude CS-MZO with (dashed line) and without (bold line) a two-trace taper, together with the modeled amplitudes (thin line).

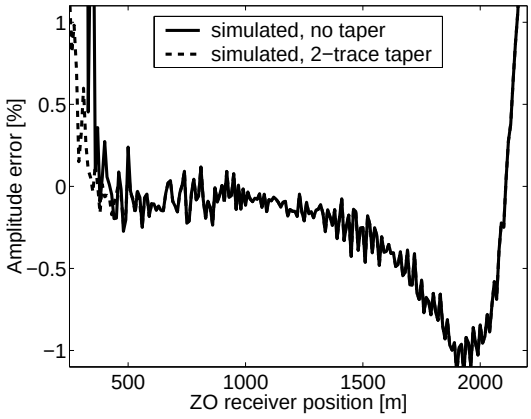

Figure 11: Amplitude error of the true-amplitude CS-MZO reflections as compared to the modeled ones.

are much better than the ones obtained from an unweighted CS-MZO (compare to Figure 14), but still remain about 40 per cent below the desired unit amplitude.

CONCLUSIONS

In this paper we have formulated a new Kirchhoff-type approach to true-amplitude shot moveout (CS-MZO) for 2.5D in-plane reflections in 2D laterally inhomogeneous media with curved interfaces. We have presented the weight functions for amplitude-preserving and true-amplitude CS-DMO and CS-MZO. Here, to preserve CS-MZO amplitudes means that output amplitudes are equal to input amplitudes, while to construct true CS-MZO amplitudes implies that in a simulated zero-offset reflection, the geometrical-spreading factor of the original common-shot reflection is replaced by the new zero-offset one for the same reflection point. This goal is achieved by a weighted one-fold single-stack integral in the time domain along specific stacking lines, the inplanats. We stress that the true-amplitude weight does not rely on any prior knowledge about the arbitrarily curved reflectors to be imaged and is theoretically valid for any reflector dip, while the amplitude-preserving weight is strictly valid for planar reflectors only. Both, the true-amplitude and the amplitude-preserving weight functions can be computed by 2D dynamic ray tracing performed along ray segments that link the two common-offset pairs of source and receivers to certain points in the macrovelocity model.

First numerical results show that true-amplitude and amplitude-preserving CS-MZO can be realized with high accuracy. In this way, zero-offset sections can be simulated directly from shot records as an alternative to the standard NMO/DMO procedure that relies on common-offset data.

ACKNOWLEDGMENTS

The research of this paper has been supported partially by the Research Foundation of the State of São Paulo (FAPESP), the National Research Council (CNPq) of Brazil, and the sponsors of the *Wave Inversion Technology (WIT) Consortium*.

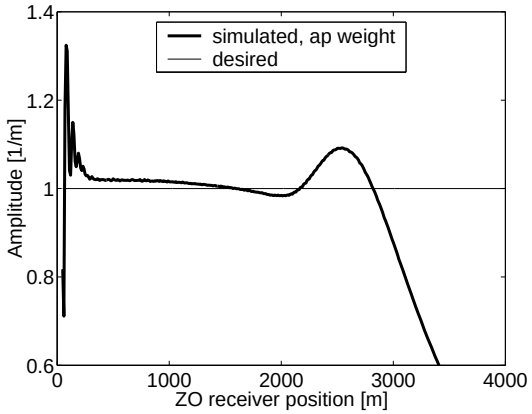

Figure 12: Picked amplitudes of the simulated zero-offset reflections resulting from an amplitude-preserving CS-MZO (bold line), together with the desired unit amplitude (thin line).

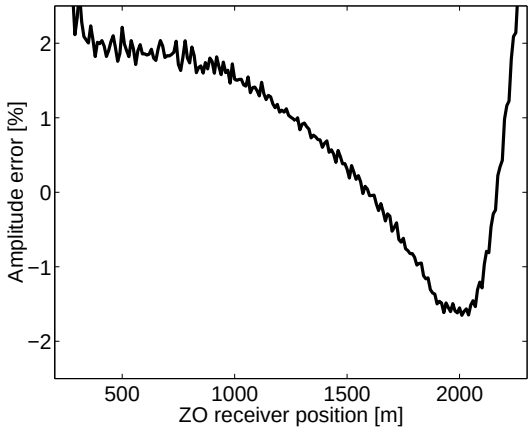

Figure 13: Amplitude error of the amplitude-preserving CS-MZO reflections as compared to the desired unit amplitude.

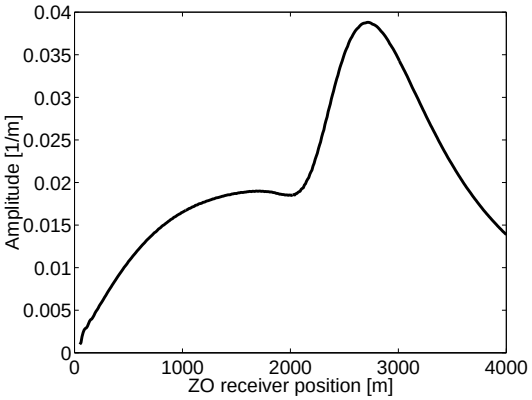

Figure 14: Picked amplitudes of the simulated zero-offset reflections resulting from an unweighted CS-MZO.

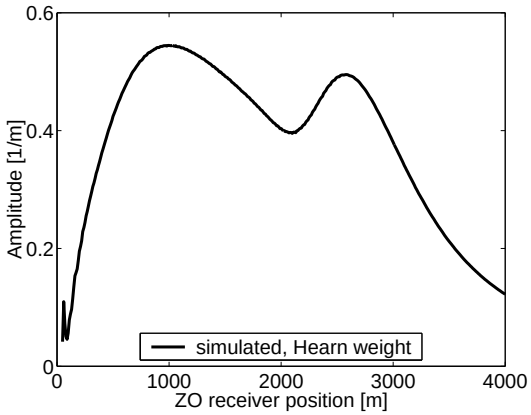

Figure 15: Picked amplitudes of the simulated zero-offset reflections resulting from a CS-MZO with Hearn's weight (corrected for the application as an MZO rather than DMO).

REFERENCES

Bagaini, C. and Spagnolini, U. (1996). 2D continuation operators and their applications. *Geophysics*, 61:1846–1858.

Beylkin, G. (1985). Imaging of discontinuities in the inverse scattering problem by inversion of a generalized Radon transform. *J. Math. Phys.*, 26(1):99–108.

Biondi, B., Fomel, S., and Chemingui, N. (1996). Application of azimuth moveout to 3D prestack imaging. In *Extended Abstracts, 66th Ann. Internat. Meeting, Soc. Expl. Geophys.*, pages 431–434, Denver.

Biondi, B. and Ronen, J. (1987). Dip moveout in shot profiles. *Geophysics*, 52:1473–1482.

Black, J., Schleicher, K., and Zhang, L. (1993). True-amplitude imaging and dip moveout. *Geophysics*, 58(1):47–66.

Bleistein, N. (1986). Two-and-one-half dimensional in-plane wave propagation. *Geophys. Prosp.*, 34:686–703.

Bleistein, N. (1987). On the imaging of reflectors in the earth. *Geophysics*, 52(7):931–942.

Bleistein, N. and Cohen, J. (1995). The effect of curvature on true-amplitude DMO: Proof of concept. *Research Note, Center for Wave Phenomena*, CWP-193.

Bleistein, N., Cohen, J., and Hagin, F. (1987). Two and one-half dimensional Born inversion with an arbitrary reference. *Geophysics*, 52(1):26–36.

Cabrera, J. and Levy, S. (1989). Shot dip moveout with logarithmic transformations. *Geophysics*, 54:1038–1041.

Canning, A. and Gardner, G. (1996). Regularizing 3D data sets with DMO. *Geophysics*, 61:1101–1114.

Červený, V. (1987). *Ray Methods for Three-Dimensional Seismic Modelling*. Petroleum Industry Course. Norwegian Institute for Technology.

Červený, V. (2001). *Seismic Ray Theory*. Cambridge University Press.

Collins, C. (1997). Imaging in 3D DMO; Part I: Geometrical optics model; Part II: Amplitude effects. *Geophysics*, 61:211–244.

Fomel, S. (1994). Method of velocity continuation in the problem of seismic time migration. *Russian Geology and Geophysics*, 35(5):100–111.

Fomel, S. and Bleistein, N. (1996). Amplitude preservation for offset continuation: Confirmation for Kirchhoff data. Technical Report CWP, Colorado School of Mines, **CWP-197**.

Granser, H. (1994). Shot gather DMO in the double log domain. *Geophysics*, 59:1305–1307.

Hearn, T. (1989). Time domain application of dip moveout to shot gather. In *Extended Abstracts, 59th Ann. Internat. Meeting, Soc. Expl. Geophys.*, pages 1140–1143.

Jaramillo, H., Schleicher, J., and Tygel, M. (1998). Discussion and errata to: "A unified approach to 3-D seismic reflection imaging, Part II: Theory" GEOPHYSICS, **61**, 759–775, 1996). *Geophysics*, 63(2):670–673.

Martins, J., Schleicher, J., Tygel, M., and Santos, L. (1997). 2.5-D true-amplitude Kirchhoff migration and demigration. *J. Seism. Expl.*, 6(2/3):159–180.

Newman, P. (1975). Amplitude and phase properties of a digital migration process. In *Abstracts, 37th Ann. Internat. Meeting, Europ. Assn. Expl. Geophys.*, Bergen. (Republished in: First Break, **8**, 397–403, 1990).

Santos, L., Schleicher, J., and Tygel, M. (1997). 2.5-D true-amplitude offset continuation. *J. Seism. Expl.*, 6(2/3):103–116.

Schleicher, J., Tygel, M., and Hubral, P. (1993). 3-D true-amplitude finite-offset migration. *Geophysics*, 58(8):1112–1126.

Tygel, M., Schleicher, J., and Hubral, P. (1994). Kirchhoff-Helmholtz theory in modelling and migration. *J. Seism. Expl.*, 3(3):203–214.

Tygel, M., Schleicher, J., and Hubral, P. (1995). Dualities between reflectors and reflection-time surfaces. *J. Seism. Expl.*, 4(2):123–150.

Tygel, M., Schleicher, J., and Hubral, P. (1996). A unified approach to 3-D seismic reflection imaging – Part II: Theory. *Geophysics*, 61(3):759–775. Errata in Jaramillo et al. (1998).

Tygel, M., Schleicher, J., Hubral, P., and Santos, L. (1998). 2.5-D true-amplitude Kirchhoff migration to zero offset in laterally inhomogeneous media. *Geophysics*, 63(2):557–573.

APPENDIX A

CONSTANT-VELOCITY MEDIUM

In this Appendix, we derive the expressions (6) and (9) for the CS-MZO stacking line and weight function in a constant-velocity medium.

CS-MZO stacking line in a constant velocity medium

A point (s_0, t_0) in the output section determines in the image space $z > 0$ the isochron $z = \mathcal{Z}_{ZO}(x; s_0, t_0)$, implicitly defined by equation (3). For a constant velocity v, equation (3) can be solved for z to yield

$$z = \mathcal{Z}_{ZO}(x; s_0, t_0) = \sqrt{R_0^2 - (x - s_0)^2}\ , \tag{18}$$

which is a half-circle with radius $R_0 = vt_0/2$ (see Figure 1). The diffraction traveltime $\mathcal{T}_D(x; s, h)$ of an arbitrary point M on the above isochron (18), i.e., $M = (x, \mathcal{Z}_{ZO}(x; s_0, t_0))$ is then given by

$$\mathcal{T}_D(x; s, h) = \frac{R_S\ +\ R_G}{v}\ , \tag{19}$$

where

$$R_S = \sqrt{(x - s)^2 + R_0^2 - (x - s_0)^2} \tag{20}$$

and

$$R_G = \sqrt{(x - s - 2h)^2 + R_0^2 - (x - s_0)^2} \tag{21}$$

are the distances from M to S and G, respectively.

With relative coordinates $X = x - s$ and $\eta = s_0 - s$, equation (19) can be recast into the form

$$\mathcal{T}_D(x; s, h) = \frac{1}{v}\sqrt{R_0^2 + 2\eta X - \eta^2} + \frac{1}{v}\sqrt{R_0^2 + 2(\eta - 2h)X + 4h^2 - \eta^2}\ . \tag{22}$$

Applying the stationary condition (5) to equation (22), we find

$$\left.\frac{\partial \mathcal{T}_D}{\partial X}\right|_{X^*} = \frac{1}{v}\,\frac{\eta}{\sqrt{R_0^2 + 2\eta X^* - \eta^2}} + \frac{1}{v}\,\frac{\eta - 2h}{2\sqrt{R_0^2 + 2(\eta - 2h)X^* + 4h^2 - \eta^2}}\ = 0\ . \tag{23}$$

From this equation, it is obvious that there can be only a stationary point if the two terms have opposite sign. Since the denominators are always positive, it follows for positive η that $\eta - 2h < 0$, i.e., $h > \eta/2$, and for negative η that $\eta - 2h > 0$, i.e., $h < \eta/2$. In other words, to construct a zero-offset trace at s_0, only traces will be needed that are recorded at receivers on the same side of s as s_0 and further away from s than s_0. Since the axis can always be chosen accordingly, we restrict our further analysis to positive η and h.

Solving equation (23) for X^*, we find the stationary point at

$$X^*(h; s_0, t_0) = \eta - R_0^2\frac{h - \eta}{\eta(2h - \eta)} = \eta + (\eta - h)\rho\ , \tag{24}$$

where we have introduced the notation

$$\rho = \frac{R_0^2}{\eta(2h - \eta)}\ . \tag{25}$$

Substitution of this result in equations (20) and (21) yields after some algebraic manipulations

$$R_S^* = \sqrt{\eta^2\,(1 + \rho)} = \eta\sqrt{1 + \rho}\ , \tag{26}$$

$$R_G^* = \sqrt{(2h - \eta)^2\,(1 + \rho)} = (2h - \eta)\sqrt{1 + \rho}\ , \tag{27}$$

where we have used that $\eta > 0$ and $2h > \eta$, as observed in connection with equation (23). With this expressions, the traveltime (19) reads

$$\begin{aligned}\mathcal{T}(h; s_0, t_0) &= \mathcal{T}_D(x^*; s, h) = \mathcal{T}_D(X^*; \eta, h)\\ &= \frac{1}{v}\,(\eta + (2h - \eta))\,\sqrt{1 + \rho} = \frac{2h}{v}\sqrt{1 + \rho}\ ,\end{aligned} \tag{28}$$

which is the expression for $\mathcal{T}$ indicated in equation (4).

CS-MZO weight function in a constant-velocity medium

To derive the constant-velocity weight function (9) from its general 2.5D representation (8), we start by discussing several geometric features that are specific to constant-velocity CS-MZO.

Curvatures of the isochrons The isochron of the zero-offset configuration is given by equation (18) and that of the common-shot configurations is a half-ellipse with the form

$$z = \mathcal{Z}_{CS}(x;s,h) = b\sqrt{1-\frac{(x-s-h)^2}{a^2}}\ , \tag{29}$$

where $a = v\mathcal{T}/2$ and $b = \sqrt{a^2-h^2}$ are the semi-axes. Therefore, we conclude from equation (28) that

$$a = h\sqrt{1+\rho} \quad \text{and} \quad b = h\sqrt{\rho}\ . \tag{30}$$

The curvatures K_0 and K of the isochrons (18) and (29) at the stationary point M^* are given by

$$K_0 = \frac{d^2\mathcal{Z}_{ZO}/dx^2}{[1+(d\mathcal{Z}_{ZO}/dx)^2]^{3/2}} = -\frac{1}{R_0} \tag{31}$$

and

$$K = \frac{d^2\mathcal{Z}_{CS}/dx^2}{[1+(d\mathcal{Z}_{CS}/dx)^2]^{3/2}} = -\frac{b}{a^2}\left(1-\frac{h^2(x-s-h)^2}{a^4}\right)^{-3/2} = -\frac{h^2}{R_0^3}\,\frac{\rho^2}{1+\rho}\ , \tag{32}$$

respectively. In formula (8) for the weight function, we need the curvature difference $K-K_0$,

$$K-K_0 \quad = \quad -\frac{h^2}{R_0^3}\,\frac{\rho^2}{1+\rho} - \frac{-1}{R_0} = \frac{1}{R_0}\left[1-\frac{h^2}{R_0^2}\,\frac{\rho^2}{1+\rho}\right]\ . \tag{33}$$

Reflection angle The law of cosines in triangle SM^*G (see Figure 1) yields

$$(2h)^2 = (R_S^*)^2 + (R_G^*)^2 - 2R_S^*R_G^*\cos 2\theta = (R_S^*+R_G^*)^2 - 4R_S^*R_G^*\cos^2\theta\ , \tag{34}$$

where R_S^* and R_G^* are given by (26) and (27). Therefore,

$$\cos^2\theta = \frac{4h^2-(R_S^*+R_G^*)^2}{-4R_S^*R_G^*} = \frac{h^2}{R_0^2}\,\frac{\rho^2}{1+\rho}\ . \tag{35}$$

Using this expression in equation (33), we can verify that

$$K-K_0 = \frac{1}{R_0}\left[1-\cos^2\theta\right] = \frac{\sin^2\theta}{R_0}\ , \tag{36}$$

which implies that $\text{sgn}(K-K_0)=1$. Thus, the last factor in weight (8) becomes

$$\exp\left\{i\frac{\pi}{2}\kappa\right\} = \exp\left\{i\frac{\pi}{4}[1-\text{sign}(K-K_0)]\right\} = 1\ . \tag{37}$$

Beylkin's determinant The 2D Beylkin determinant is defined as

$$h_B = \det\begin{pmatrix} \dfrac{\partial}{\partial x}\mathcal{T}_D(x,z;h) & \dfrac{\partial}{\partial z}\mathcal{T}_D(x,z;h) \\[2ex] \dfrac{\partial^2}{\partial x\partial h}\mathcal{T}_D(x,z;h) & \dfrac{\partial^2}{\partial z\partial h}\mathcal{T}_D(x,z;h) \end{pmatrix}\ , \tag{38}$$

where

$$\mathcal{T}_D(x,z;h) = \frac{1}{v}\sqrt{(x-s)^2+z^2} + \frac{1}{v}\sqrt{(x-s-2h)^2+z^2}\ . \tag{39}$$

All these quantities are taken at the stationary point $M^* = (x^*, z^*)$ with

$$z^* = \mathcal{Z}_{CS}(x^*; h, t) = \mathcal{Z}_{ZO}(x^*; s_0, t_0) = \sqrt{R_0^2(1+\rho) - h^2\rho^2}\ . \tag{40}$$

With the help of the stationary value (24) and the formulas (26) and (27) for R_S^* and R_G^*, the above determinant (38) reduces to

$$|h_B| = \frac{4h^2\rho\sqrt{R_0^2(1+\rho) - h^2\rho^2}}{v^2(2h-\eta)^3\eta(1+\rho)^2}\ . \tag{41}$$

Geometrical-spreading factors In a constant-velocity medium, the out-of-plane Fresnel factors $\mathcal{L}_F$ and $\mathcal{L}_{F0}$ have the simple form

$$\mathcal{L}_F = \left(\frac{1}{vR_S^*} + \frac{1}{vR_G^*}\right)^{-1/2} = (1+\rho)^{1/4}\sqrt{\frac{v\eta(2h-\eta)}{2h}}\ , \tag{42}$$

and

$$\mathcal{L}_{F0} = \left(\frac{1}{vR_0} + \frac{1}{vR_0}\right)^{-1/2} = \sqrt{\frac{vR_0}{2}}\ . \tag{43}$$

Also, the point-source geometrical spreading factors are just the distances from the source or receiver. In other words, $\mathcal{L}_0 = R_0$, $\mathcal{L}_S = R_S^*$, and $\mathcal{L}_G = R_G^*$.

Final weight function We are now in the position of actually computing the weight function $\mathcal{W}(h; s_0, t_0)$ for a constant velocity medium. Collecting the above intermediate results, we finally arrive at

$$\begin{aligned}\mathcal{W}(h; s_0, t_0) &= \left(\frac{v}{2}\right)^{3/2}(1+\rho)^{3/4}\sqrt{\frac{h}{R_0\rho}}\ \frac{R_0^2(1+\rho)}{h^2\rho^2}\ \frac{4h^2\rho^2}{v^2(2h-\eta)^2(1+\rho)^{3/2}\sqrt{R_0}} \\ &= \sqrt{\frac{2h}{v}}\sqrt{1+\rho}\ \frac{R_0}{\sqrt{\rho}}\ \frac{1}{(2h-\eta)^2}\ .\end{aligned} \tag{44}$$

Under the first square root, we recognize $\mathcal{T}$ as given in equation (28). Upon the use of equation (25), the weight function (44) can then be recast into the form of equation (9).

Aperture consideration

To determine the aperture A to be used in stack (1), we use the condition that the stationary point X^* as given by equation (24) must be located on the real extension of the zero-offset isochron (18). This translates into the mathematical restriction

$$\eta - R_0 < X^* < \eta + R_0\ . \tag{45}$$

Substitution of equation (24) leads, because $\eta > 0$ and $2h - \eta > 0$, to the condition

$$R_0|h - \eta| < \eta(2h - \eta)\ . \tag{46}$$

Here, we must distinguish two cases:
(A) For $h \geq \eta$, condition (46) yields the following conditions on h:

$$\begin{array}{rcccll} \eta & \leq & h & < & \dfrac{\eta(R_0-\eta)}{R_0-2\eta} & \text{for } R_0 > 2\eta \\ \eta & \leq & h & < & \infty & \text{for } R_0 \leq 2\eta\ . \end{array} \tag{47}$$

(B) For $h < \eta$, condition (46) yields

$$h > \frac{\eta(R_0+\eta)}{R_0+2\eta}\ . \tag{48}$$

The condition that h must be larger than $\eta/2$ is implicitly satisfied by inequality (48). The combination of results (47) and (48) yields the aperture condition as stated in equation (17).